JGR Space Physics

RESEARCH ARTICLE
10.1029/2021JA030230

Multi-Scale Density Structures in the Plasmaspheric Plume During a Geomagnetic Storm

Y. Nishimura[1], J. Goldstein[2,3], C. Martinis[4], Q. Ma[4,5], W. Li[4], S. R. Zhang[6], A. J. Coster[6], S. Mrak[7], J. L. Semeter[1], N. Nishitani[8], J. M. Ruohoniemi[9], and S. G. Shepherd[10]

[1]Department of Electrical and Computer Engineering and Center for Space Physics, Boston University, Boston, MA, USA, [2]Space Science and Engineering Division, Southwest Research Institute, San Antonio, TX, USA, [3]Department of Physics and Astronomy, University of Texas, San Antonio, TX, USA, [4]Department of Astronomy and Center for Space Physics, Boston University, Boston, MA, USA, [5]Department of Atmospheric and Oceanic Sciences, University of California, Los Angeles, CA, USA, [6]MIT Haystack Observatory, Westford, MA, USA, [7]Space Weather Technology, Research and Education Center, University of Colorado Boulder, Boulder, CO, USA, [8]Institute for Space Earth Environmental Research, Nagoya University, Nagoya, Japan, [9]Bradley Department of Electrical and Computer Engineering, Virginia Tech, Blacksburg, VA, USA, [10]Thayer School of Engineering, Dartmouth College, Hanover, NH, USA

Key Points:

- Two dimensional structure and motion of fine-scale plume density has been revealed by Van Allen Probes-defense meteorological satellite program-Swarm-global positioning system conjunction
- Fine-scale subauroral polarization streams flows are related to fine-scale density and are suggested to create turbulent density cascading
- Fine-scale density contributes to waves, precipitation, heating, and scintillation

Correspondence to:
Y. Nishimura,
toshi16@bu.edu

Citation:
Nishimura, Y., Goldstein, J., Martinis, C., Ma, Q., Li, W., Zhang, S. R., et al. (2022). Multi-scale density structures in the plasmaspheric plume during a geomagnetic storm. *Journal of Geophysical Research: Space Physics*, *127*, e2021JA030230. https://doi.org/10.1029/2021JA030230

Received 20 DEC 2021
Accepted 15 MAR 2022

Author Contributions:
Conceptualization: Y. Nishimura, J. Goldstein
Data curation: J. Goldstein, Q. Ma, W. Li, S. R. Zhang, A. J. Coster, S. Mrak, N. Nishitani, J. M. Ruohoniemi, S. G. Shepherd
Formal analysis: Y. Nishimura, J. Goldstein
Funding acquisition: Y. Nishimura, Q. Ma, W. Li, J. L. Semeter
Investigation: Y. Nishimura, J. Goldstein, C. Martinis
Methodology: Y. Nishimura, J. Goldstein, S. R. Zhang, A. J. Coster, S. Mrak, J. L. Semeter, N. Nishitani, J. M. Ruohoniemi, S. G. Shepherd
Project Administration: Y. Nishimura
Resources: J. Goldstein, Q. Ma, W. Li
Software: Y. Nishimura, J. Goldstein, S. R. Zhang, A. J. Coster, S. Mrak, N. Nishitani, J. M. Ruohoniemi, S. G. Shepherd
Supervision: Y. Nishimura

Abstract Evolution of large-scale and fine-scale plasmaspheric plume density structures was examined using space-ground coordinated observations of a plume during the 7–8 September 2015 storm. The large-scale plasmaspheric plume density at Van Allen Probes A was roughly proportional to the total electron content (TEC) along the satellite footprint, indicating that TEC distribution represents the large-scale plume density distribution in the magnetosphere. The plasmaspheric plume contained fine-scale density structures and subauroral polarization streams (SAPS) velocity fluctuations. High-resolution TEC data support the interpretation that the fine-scale plume structures were blobs with ~300 km size and ~500–800 m/s in the ionosphere (~3,000 km size and ~5–8 km/s speed in the magnetosphere), emerging at the plume base and drifting to the plume. The short-baseline Global Navigation Satellite System receivers detected smaller-scale (~10 km in the ionosphere, ~100 km in the magnetosphere) TEC gradients and their sunward drift. Fine-scale density structures were associated with enhanced phase scintillation index. Velocity fluctuations were found to be spatial structures of fine-scale SAPS flows that drifted sunward with density irregularities down to ~10 s of meter-scale. Fine-scale density structures followed a power law with a slope of ~−5/3, and smaller-scale density structures developed slower than the larger-scale structures. We suggest that turbulent SAPS flows created fine-scale density structures and their cascading to smaller scales. We also found that the plume fine-scale density structures were associated with whistler-mode intensity modulation, and localized electron precipitation in the plume. Structured precipitation in the plume may contribute to ionospheric heating, SAPS velocity reduction, and conductance enhancements.

Plain Language Summary A plume of cold plasma circulates in the system during geomagnetic storms, and it is important for global positioning system (GPS) signal scintillation at mid-latitudes of the Earth. We show that the plume contains fine-scale density structures across multiple-scales, and reveal their 2-d structure and motion using GPS remote sensing and multiple satellites. The network of GPS receivers showed that the fine-scale plume structures were blobs with hundreds of km size in the ionosphere, and GPS signal scintillation was highly correlated with the fine-scale density structures. Radar observations identified a close relation between the fine-scale density and fast plasma streams. The plume density structures formed first at large-scales and then small-scale density structures emerged near the peak of the geomagnetic storm. We suggest that fast plasma streams created fine-scale density structures and their turbulent cascading to smaller scales.

1. Introduction

The plasmaspheric plume is an important density structure of cold plasma in the magnetosphere-ionosphere coupled system during geomagnetically disturbed times. Remote sensing by extreme ultraviolet imaging and global positioning system (GPS) total electron content (TEC) has been widely used to characterize the large-scale structure and evolution of the plume (e.g., Foster et al., 2002, 2014; Goldstein & Sandel, 2005). In situ

Validation: Y. Nishimura, J. Goldstein, S. R. Zhang, A. J. Coster, S. Mrak, N. Nishitani, J. M. Ruohoniemi, S. G. Shepherd
Visualization: Y. Nishimura, J. Goldstein
Writing – original draft: Y. Nishimura
Writing – review & editing: J. Goldstein, C. Martinis, Q. Ma, W. Li

measurements of the cold plasma density have revealed that the plasmaspheric plume always contains fine-scale density structures (Goldstein et al., 2004; Spasojević et al., 2003). The amplitude of fine-scale density structures can be larger than the large-scale density, and thus the fine-scale density structures have significant contributions to cold plasma structures in the plume. The size of the fine-scale structures in the magnetosphere is of the order of 1,000 km (Moldwin et al., 1995). Smaller-scale structures may also exist, but are difficult to measure because of limited instrument sampling rates.

The sunward motion of the plume is driven by the enhanced convection that includes large-scale convection and the subauroral polarization streams (SAPS) (Goldstein & Sandel, 2005). Interestingly, the velocity in the fine-scale density structures is not smooth but has large-amplitude velocity fluctuations (Borovsky & Denton, 2008; Goldstein et al., 2004). While it is possible that the velocity fluctuations are instrumental noise, if they are real velocity features, the velocity fluctuations could be turbulent flows that create the fine-scale density structures. However, it is not understood whether the velocity fluctuations are spatial or temporal. If the velocity fluctuations are spatial, their scale size and speed should be compared to the size and motion of the fine-scale density structures in order to examine whether the velocity fluctuations contribute to the formation of the fine-scale density structures. Goldstein et al. (2004) and Borovsky and Denton (2008) also discussed that other mechanisms could create the fine-scale density structures: The fine-scale density structures may originally exist in the plasmasphere and be transported by the enhanced convection. Gradient drift instability, velocity shear, and magnetosphere-ionosphere coupling time scales (such as the Alfven transit time) could also be candidates for the formation of the fine-scale structures. These possibilities should also be tested to identify the potential mechanism for creating the fine-scale density structures.

It is difficult to evaluate these potential mechanisms for the fine-scale density structures using single-satellite observations. The Cluster satellites have been used to show that the plume density structures are spatial (Matsui et al., 2012). However, the density structures they measured were stationary, and it is not understood whether the density structures in enhanced convection are spatial or temporal. It is even more challenging to determine the origin of the fine-scale density structures because a wide spatial and temporal coverage is required to trace motion of the fine-scale density structures.

Ionospheric observations have been widely used for plume and SAPS research owing to the advantage of 2-d measurement capability. GPS receivers have been used to show that density irregularities are present in the plume (Heine et al., 2017; Mrak et al., 2020). The plume can evolve to multiple channels and density irregularities are localized to their steep TEC gradients (Nishimura et al., 2021). Super Dual Auroral Radar Network (SuperDARN) echoes are also enhanced at the TEC gradients, indicating that density irregularities extend down to 10s of meter wavelengths (Nishimura et al., 2021). Velocity observations in the ionosphere have shown that SAPS also contain fine-scale (~tens of km) structures that propagate quasi-periodically (Erickson et al., 2002; Foster et al., 2004; Makarevich & Bristow, 2014; Oksavik et al., 2006). Such flows are wave-like structures in the broader SAPS flow channel and are associated with density irregularities (Mishin & Blaunstein, 2008; Mishin & Burke, 2005). Although ionosphere observations have not been used to identify 2-d structures and motion of fine-scale density structures in the plume, their wide coverage could be used to address what the 2-d structures of the fine-scale density structures are, where they are created, whether they move with flow fluctuations, and whether the flow fluctuations are spatial or temporal.

The present paper addresses these fundamental questions on the fine-scale structures in the plume, by utilizing a coordinated observation event of the plume in the magnetosphere and ionosphere during the 7–8 September 2015 geomagnetic storm. Van Allen Probes A (RBSP-A) encountered the plume in the inner magnetosphere during the storm main phase, and the GPS network detected the plume in the ionosphere at multiple scales. The GPS TEC observations provided critical information of 2-d distribution and motion of the fine-scale density structures. The Defense Meteorological Satellite Program (DMSP) and Swarm satellites were located near the local time of RBSP-A and were used to complement the TEC observations. One of the SuperDARN radars provided 2-d observations of the velocity fluctuations and density irregularities. This dataset was also used to examine whether the fine-scale density impacts whistler-mode waves and precipitation. We also evaluate whether motion of the plume density is mainly due to convection, or whether substantial upflow/outflow is present in the plume.

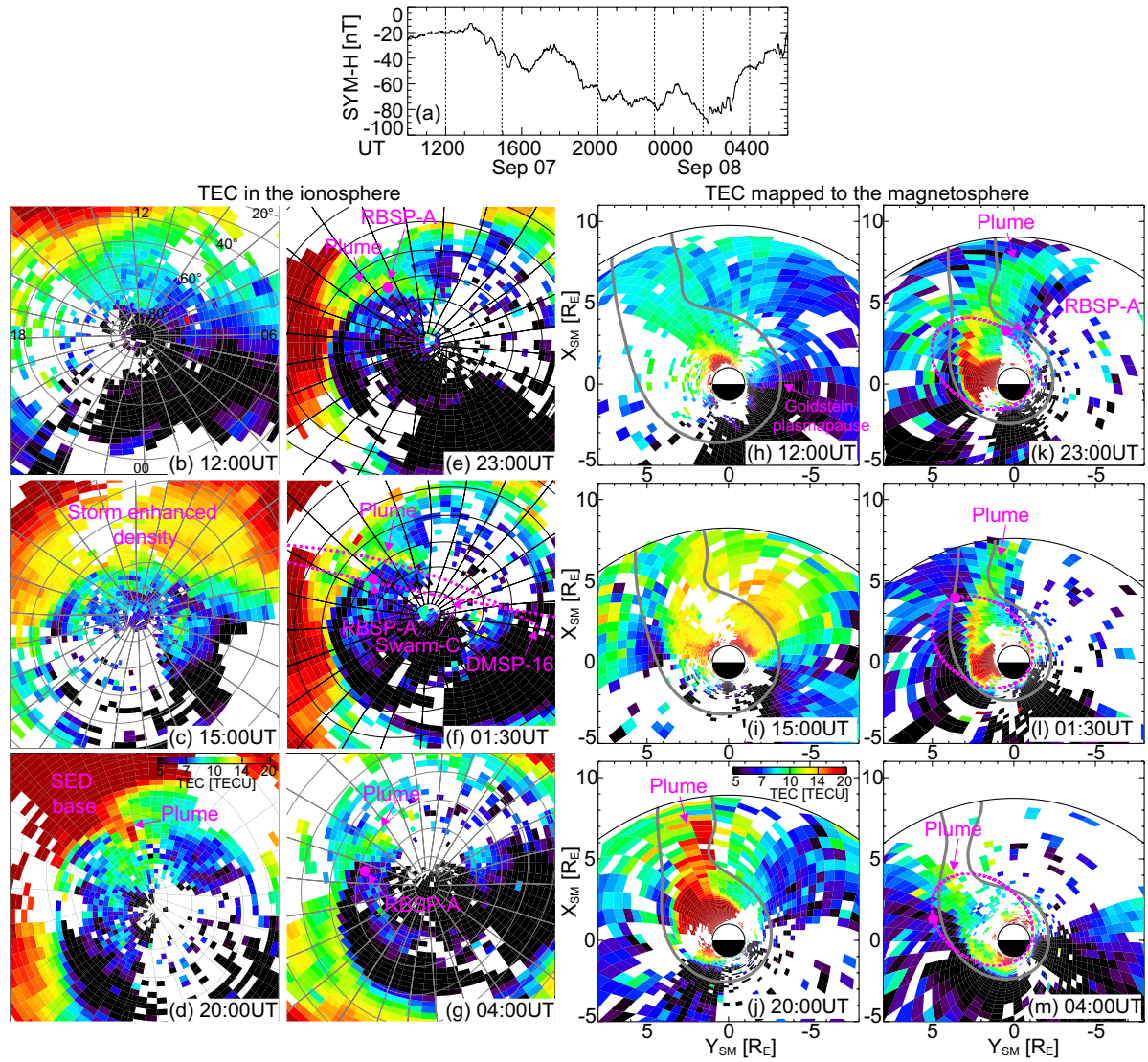

Figure 1. (a) SYM-H index for the 7–8 September 2015 storm. The vertical lines mark the times of the total electron content (TEC) maps. (b–g) TEC maps in the ionosphere in the northern hemisphere on 2° geographic latitude and 6° longitude grids. (h–m) TEC maps projected to the equatorial plane along the T01 magnetic field model. The magenta dot shows the Van Allen Probes A (RBSP-A) location. The magenta lines show the satellite orbits. The gray envelope in Panels (h–m) shows the simulated plasmapause (Goldstein et al., 2014). The black line in Panels (h–m) marks the model magnetopause (Shue et al., 1998).

2. Results

2.1. Large-Scale Plume Structure

The main phase of the storm took place between ~13:00 UT on 7 September 2015 and ~02:00 UT on 8 September 2015 (Figure 1a). Figures 1b–1g show TEC maps in the northern hemisphere at selected times that are indicated in Figure 1a. TEC data were gridded to 2° geographic latitude and 6° longitude cells with 5 min time resolution. TEC increased in the dayside mid-latitude ionosphere during the early main phase, known as storm enhanced density (SED, Figure 1c). Then a narrow plume formed at ~13–14 hr magnetic local time (MLT, Figure 1d), and the plume base rotated toward the dusk in the late main phase (Figures 1e and 1f). The plume TEC decreased in the recovery phase (Figure 1g). This large-scale plume evolution is consistent with the repeatable pattern of the plume dynamics documented by Goldstein and Sandel (2005).

The TEC maps were projected to the equatorial plane by tracing the T01 magnetic field lines (Tsyganenko, 2002) (Figures 1h–1m). Different magnetic field models provide essentially the same mapping of the plume. The dark

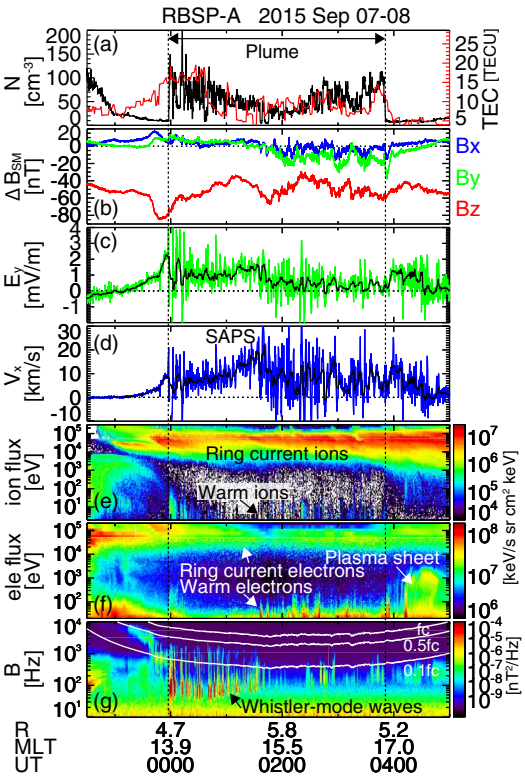

Figure 2. Van Allen Probes A (RBSP-A) observations during the storm. (a) Total plasma density, (b) magnetic field in the solar magnetic (SM) coordinates (a quiet-time background has been subtracted), (c) dawn-to-dusk electric field in modified Geocentric solar ecliptic, (d) sunward $E \times B$ drift speed, (e) ion energy flux perpendicular to the magnetic field, (f) electron energy flux perpendicular to the magnetic field, and (g) wave magnetic field spectrogram. The black lines in Panels c–d are 5-min smoothed data. The red line in Panel a is total electron content (TEC) along the RBSP-A orbit mapped to the ionosphere. The white lines in Panel g are fractions of the local electron cyclotron frequencies. The vertical lines indicate the sunward and anti-sunward edges of the plasmaspheric plume.

gray envelope was produced by a simulated plasmapause by the plasmapause test particle (PTP) model (Goldstein et al., 2014). The PTP simulation run for this event was initialized at 00:00 UT on 7 September 2015 with an initial plasmapause specified by the empirical model of O'Brien and Moldwin (2003) and driven in 10-s time steps by Kp and the OMNI solar wind electric field with scaling factor $f = 0.2$ (Goldstein et al., 2014). Consistent with the TEC data, the PTP model also predicted that the plume was wide in the early main phase (Figure 1i). The simulated plume became narrower (Figure 1j) and then rotated duskward (Figure 1m). Although the simulated plume was shifted duskward of the TEC plume by ~1–2 R_E, PTP reasonably reproduced the overall behavior of the plume of this event. The difference between the PTP and TEC plumes could be because the PTP simulation uses a simplified initial plasmapause location and convection electric field model.

The magenta dot in Figures 1e–1g and 1k–1m indicates the RBSP-A location. RBSP-A encountered the TEC plume at ~23 UT (late main phase) and stayed close to the plume until ~4 UT (early recovery phase). The RBSP-A data are shown in Figure 2. Based on the in-situ density from the upper-hybrid resonance frequency (black line in Figure 2a), RBSP-A encountered the plasmaspheric plume at 23:58 UT and left the plume at 03:51 UT. The RBSP-A orbit was traced to the ionosphere, and the TEC data nearest to the RBSP-A footprint were recorded and are shown as the red line in Figure 2a. To retain the original resolution of the TEC data, ungridded TEC maps (1-min resolution at each ionosphere pierce point, see Section 2.4 for more details) were used instead of the gridded TEC in Figure 1. The sunward edge of the TEC plume was more gradual, and RBSP-A encountered the TEC plume somewhat earlier than the plasmaspheric plume (the steepest TEC gradient was found at 23:47 UT). The anti-sunward edge of the TEC plume coincided well with that of the plasmaspheric plume within a few minutes of difference. Both the plasmaspheric plume density and TEC were elevated near the edges of the plume and were reduced near the middle of the plume (~2 UT). In this event, TEC and the in-situ density approximately followed a scaling that is described as $n = 8.1TEC - 31$ [cm^{-3}]. This relation indicates that TEC in the plume reasonably represents the plasmaspheric plume density with an appropriate scaling. In addition to the large-scale plume structure, the plume also had notable fine-scale density structures, consistent with the observations by Goldstein et al. (2004). The fine-scale density structures are investigated in detail in Sections 2.2–2.4.

As typical storm-time features, the B_z magnetic field in the inner magnetosphere was reduced due to the enhanced ring current (Figure 2b), and the E_y electric field was enhanced (Figure 2c). The $E \times B$ drift speed for the measured electric field (using both E_y and E_z) was enhanced sunward (Figure 2d), where the averaged sunward drift speed in the plume was 8.4 km/s. The enhanced ring current ions (>keV) can be seen on the same field lines as the plume (Figure 2e), and its leading edge coincided with the encounter of the enhancement of E_y. The inner edge of the electron plasma sheet (<~3 keV) was not found until 04:11 UT (Figure 2f), and thus the plume was located on subauroral magnetic field lines and the enhanced sunward drift was the magnetospheric signature of the SAPS. Warm ion and electron fluxes were also enhanced intermittently below a few 100 eV. Whistler-mode waves also intensified in the plume (Figure 2g), consistent with the earlier finding by Yuan et al. (2012) and Li et al. (2019), where the plume density increases the growth rate of whistler-mode waves and forms a duct for wave propagation (Chen et al., 2012).

Another notable feature in Figures 2c and 2d is that the electric field and hence the $E \times B$ drift speed had large-amplitude fluctuations. The fluctuations started when the satellite encountered the plume, and they were well above the noise level (~0.1 mV/m). This observation supports that the flow fluctuations that were suggested by Goldstein et al. (2004) are real flow features in the plume, and that the flow fluctuations could contribute to

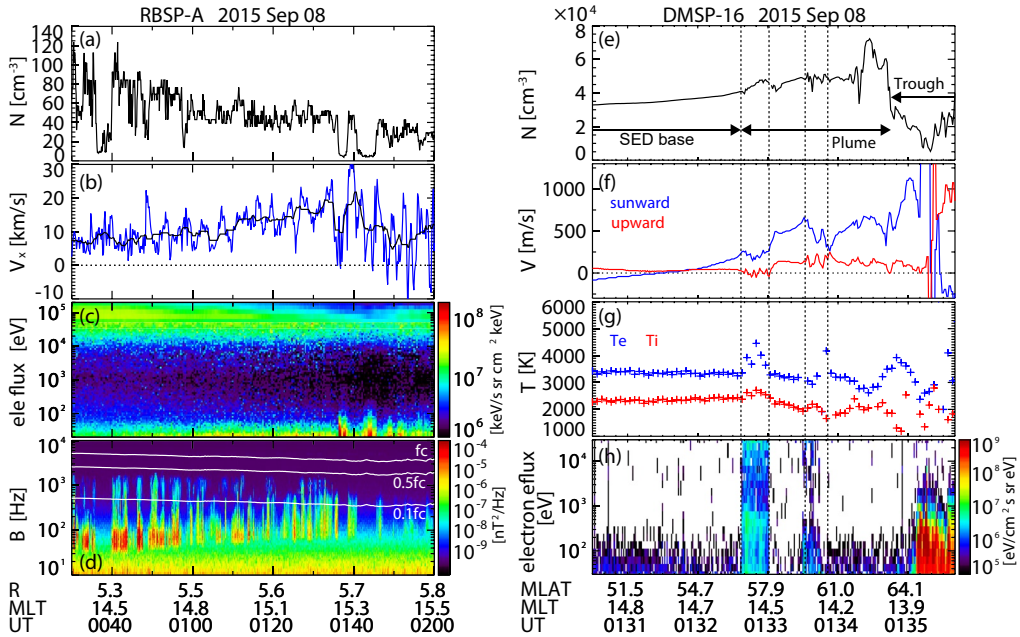

Figure 3. (Left) Van allen probes A (RBSP-A) observations over 00:30–02:00 UT. (a) Total plasma density, (b) sunward $E \times B$ drift speed, (c) electron energy flux, and (d) wave magnetic field spectrogram. (Right) defense meteorological satellite program (DMSP-16) observations over 01:30:30–01:35:40 UT. (e) Total plasma density, (f) sunward and upward velocities, (g) ion and electron temperatures, and (h) precipitating electron energy flux.

the formation of fine-scale density structures in the plume. The relation between the flow fluctuations and plume density is examined further in Sections 2.2 and 2.5.

2.2. Fine-Scale Plume Density and Electron Precipitation

Figures 3a–3d show a blowup of the RBSP-A observations within the plume between 00:30–02:00 UT. The plume contained fine-scale density structures, where the characteristic size was a few minutes or ∼2,000 km length at ∼10 km/s speed (Figure 3a). The amplitude of the fine-scale density perturbations was comparable to or larger than the large-scale plume density. The sunward $E \times B$ drift also fluctuated substantially, and the fluctuation amplitude was comparable to the smoothed velocity (Figure 3b). Both density and velocity fluctuations had a major period of ∼5 min, indicating a potential physical connection between the density and velocity fluctuations. The phase lag, however, was not constant but variable (out-of-phase in the first few tens of minutes, and then in-phase). The whistler-mode waves were enhanced in the regions of density enhancements, and the wave intensity was correlated with the density (Figure 3d). The electron flux above 10 keV only slowly changed in time without a correlation with the density, while the low-energy electrons below 100 eV were enhanced in some of the density depletions (Figure 3c). Thus, the whistler-mode wave intensifications were not due to changes in energetic electron fluxes but due to the modulation of the plume plasma density.

Around 01:33 UT, DMSP-16 passed the plume ∼1 hr MLT away from the footprint of RBSP-A (Figure 1f). DMSP detected the plume at 01:32:40–01:34:45 UT in the sunward flow (Figures 3e and 3f). The equatorward boundary of the auroral oval was located at 01:35:07 UT. Thus, consistent with the RBSP-A observations, the plume was indeed present in the subauroral ionosphere and the sunward flow was SAPS. The upward flow was also measured in the plume, but its magnitude (∼200 m/s) was much less than the sunward flow. Therefore, the plume plasma was dominantly transported sunward perpendicular to the magnetic field. Unless large upward accelerations occur above the topside ionosphere, the plume plasma at the DMSP location would not reach the RBSP-A location but would go much farther downstream of the convection.

The plume along the DMSP orbit also had significant fluctuations of the density and SAPS flow speed. Interestingly, electron precipitation and ionospheric electron temperature were enhanced in two of the regions of velocity reductions and density enhancements (Figures 3g and 3h, highlighted by the dashed lines). The precipitating

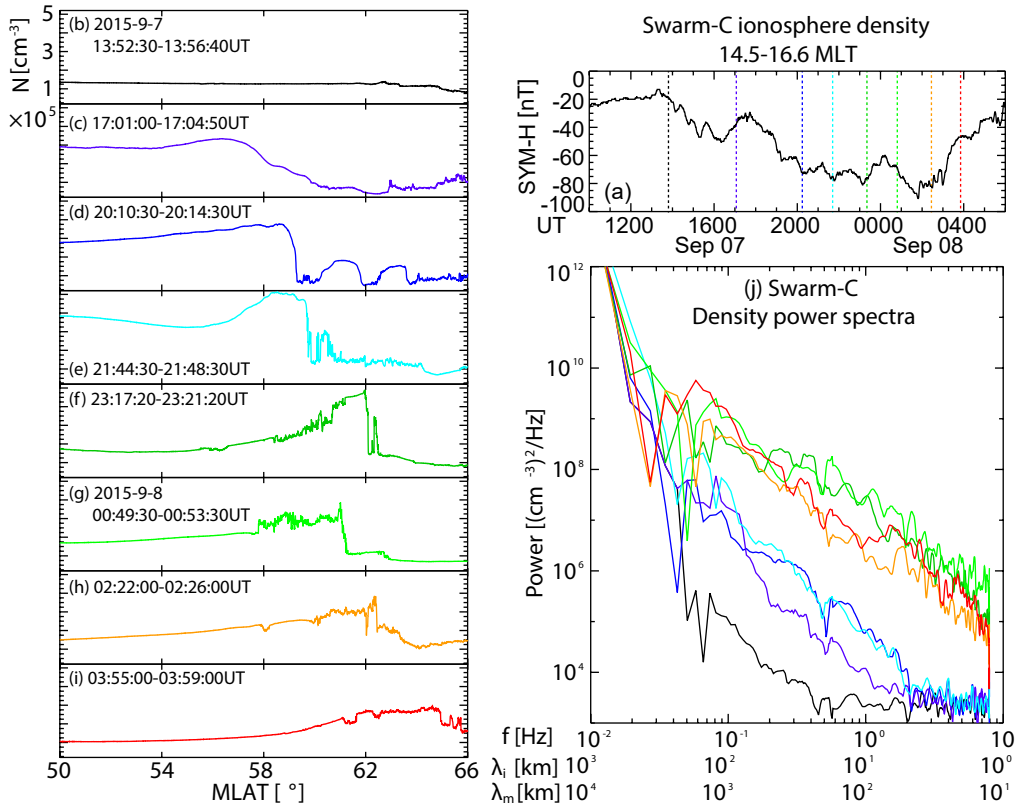

Figure 4. (a) SYM-H and the times of the Swarm-C observations, (b–i) density observations along the selected passes of Swarm-C in the northern hemisphere on the dusk side (14.5–16.6 hr magnetic local time), and (j) power spectra of the density. The conversion to the wavelength is obtained based on 7.8 km/s satellite orbital speed and the magnetosphere-ionosphere mapping factor of ~10.

electrons spread over a wide energy range without inverted-V spectra, and thus the precipitation was likely driven by wave-particle interaction. The >10 keV precipitation could arise from scattering of the >10 keV electrons in the inner magnetosphere (Figure 3c) by the whistler-mode waves (Figure 3d), similar to the results shown in Li et al. (2019). Because the >10 keV electrons in the inner magnetosphere only changed slowly, the precipitation structures may reflect wave structures associated with the plume density fluctuations that were described earlier (Figures 3a and 3d; though we cannot directly see the connection because the satellites were not exactly on the same field lines). The <keV flux in the inner magnetosphere was low and thus acceleration along the magnetic field lines is required to explain the <keV precipitation.

The precipitation is likely the cause of the ionospheric plasma heating. The reduction of the SAPS flow could be because the precipitation increased the ionospheric conductance. The ionospheric heating and SAPS velocity modulation suggest that precipitation in the plume has significant impacts onto the subauroral ionosphere. Note that electron temperature was also elevated in another velocity reduction and density enhancement at ~01:34:50 UT, but precipitation was not enhanced within the measurable energy range.

2.3. Multi-Scale Plume Density From Swarm

The Swarm satellites passed the plume multiple times during the storm and provided time evolution of the plume density structure. Eight of the Swarm-C satellite passes were selected during the main and early recovery phases (Figure 4a), and the density for each satellite pass is shown in Figures 4b–4i. The orbit of Swarm-C was close to that of DMSP-16 and the footprint of RBSP-A (Figure 1f). The density at the beginning of the main phase was low and nearly uniform without the plume (Figure 4b). The plume became evident with the storm enhanced density as the main phase progressed (Figures 4c–4f). The equatorward boundary of the trough also became steeper in time. Localized density structures also developed poleward of the main plume density enhancement,

and they could also be part of the structured plume density. The plume density became lower and the density peak moved poleward during the early recovery phase (Figures 4h and 4i).

In addition to the large-scale plume, fine-scale density structures developed during the storm main phase. The plume density in the early main phase was dominated by the large-scale structure (Figures 4b–4e), but then the plume showed density irregularities in the late main phase particularly in the equatorward portion of the plume (Figures 4f and 4g). The irregularities became weaker but still existed in the early recovery phase (Figures 4h and 4i). The power spectra of the plume density in Figure 4j present time-evolution of the density at various scales. The horizontal axis shows the wavelengths in the ionosphere and magnetosphere assuming that Swarm-C measured spatial structures. The satellite velocity (∼7.8 km/s) was much faster than the plasma flow velocity (<∼1 km/s, Figure 3f and Section 2.5), and as shown later, the motion of the plume density was mainly azimuthal. Thus, the variations in the satellite frame of reference were approximately spatial. At large-scales (>∼500 km in the ionosphere), the spectral power became the largest in the early main phase. At meso-scales (∼100 km), the spectral power increased as the storm progressed and became the largest in the recovery phase. The spectral power at small-scales (<∼100 km) also increased during the main phase and peaked near the end of the main phase. While the spectra at <∼100 km size followed a power law, the spectral slope became less steep as the time progressed. A spectral break was initially at ∼20 km size (beginning of the main phase), and then shifted to ∼5 km (early main phase) and <1 km (late main and early recovery phases). This time evolution of the spectra indicates that the density irregularities developed at longer wavelengths first and then shorter-wavelength irregularities developed afterwards. Considering that the spectra followed a power law, it is likely that turbulence developed in the plume and that the density structures cascaded down to smaller scales as the storm developed.

2.4. Multi-Scale Plume Density From TEC

In order to determine the 2-d structure of the fine-scale plume density, we used high-resolution vertical TEC maps at individual lines-of-sight (LOS) between the GPS receivers and satellites every minute. Figures 5a–5c show three selected snapshots of the high-resolution TEC maps in North America near the end of the main phase. This region covered the plume and RBSP-A footprint in the afternoon sector (Figure 1). Interestingly, TEC along the plume had multiple TEC enhancements (fine-scale TEC structures) as highlighted by the magenta arrows. The fine-scale TEC structures were quasi-periodic blobs in the plume and the poleward edge of the SED base. TEC farther toward midnight or at lower latitudes did not have such fine-scale structures, and thus the fine-scale TEC structures did not originate near midnight or at lower latitudes.

The rate of TEC index (ROTI), a measure of ionospheric irregularities, also shows that temporal variations of TEC were locally enhanced at the plume base and in the plume as highlighted by the magenta dotted line (Figures 5d–5f). ROTI in the plume can be as large as those in the auroral oval (elevated ROTI poleward of the plume), and thus the TEC variations in the plume were comparable to those in the auroral oval.

TEC along the plume is plotted as a function of magnetic longitude (MLON) in Figure 6b. Here, background TEC was removed by subtracting minimum TEC within each 30 min sliding window (ΔTEC) (Zhang et al., 2019). ΔTEC in central Alaska is also plotted as a function of magnetic latitude (MLAT) in Figure 6c. ΔTEC in the plume had fine-scale structure that drifted sunward repetitively. Although coverage gaps occasionally appeared at ∼−80° MLON, the fine-scale structures were seen to form mostly at the base of the plume, and ΔTEC away from the plume base (>∼−60° MLON) was mostly smooth. The emergence of the fine-scale structures in the plume base provides evidence that the fine-scale structures formed at the plume base and drifted into the plume. It is unlikely that such fine-scale structures were present in the quiet-time density structure and became the fine-scale structure by convection. This finding is consistent with the suggestion that there were less structures in the main plasmasphere (Spasojević et al., 2003). The characteristic size of the quasi-periodic structure was ∼300 km, and the drift speed was ∼500–800 m/s, based on the size and motion of ΔTEC in Figure 1e. This speed was comparable to the sunward drift speed measured by DMSP-16 (Figure 3f), and thus the fine-scale structures drift at the $E \times B$ velocity. Figure 6c also shows that the TEC enhancements can be seen as quasi-periodic TEC modulation at a fixed longitude only within the plume latitudes, with an apparent poleward and equatorward expansion because of a blob drifting across the longitude. The size and speed in the ionosphere corresponded to a ∼3,000 km size and ∼5–8 km/s speed in the inner magnetosphere by tracing the magnetic field lines (the mapping factor is ∼10). This size is consistent with the estimate from the in-situ density (Moldwin et al., 1995). This range of speed is

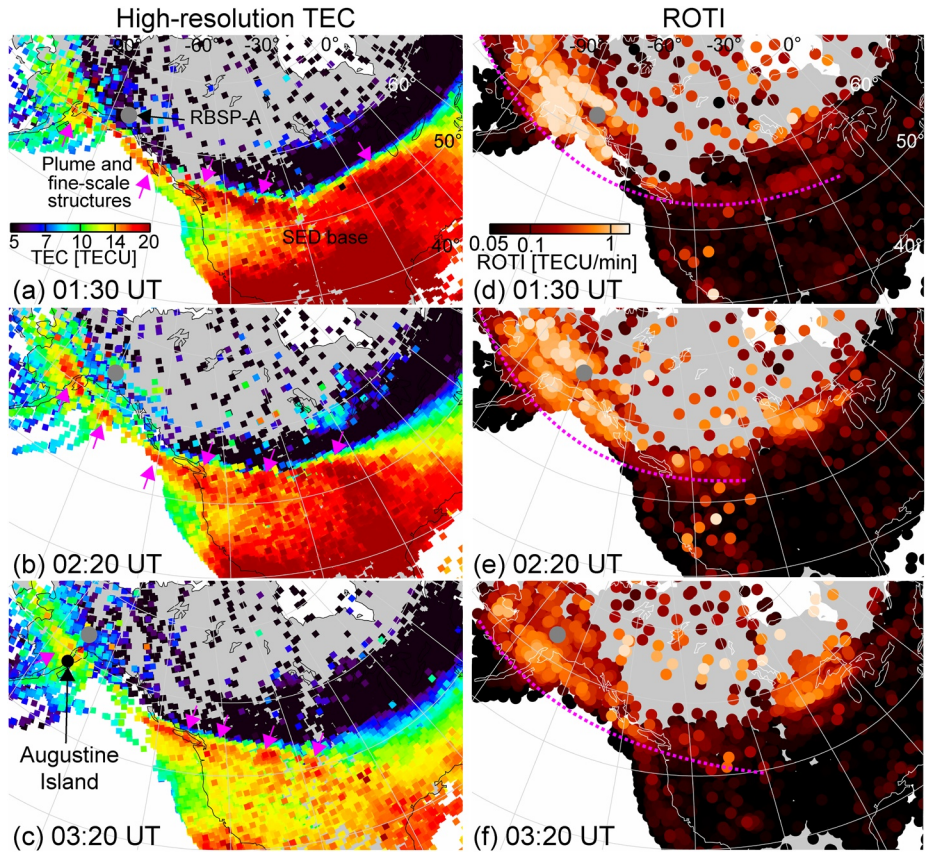

Figure 5. Selected (a–c) high-resolution total electron content and (d–f) rate of TEC index maps in North America at 01:30, 02:20 and 03:20 UT on 8 September 2015. The Van Allen Probes A footprint is overlaid as a gray dot.

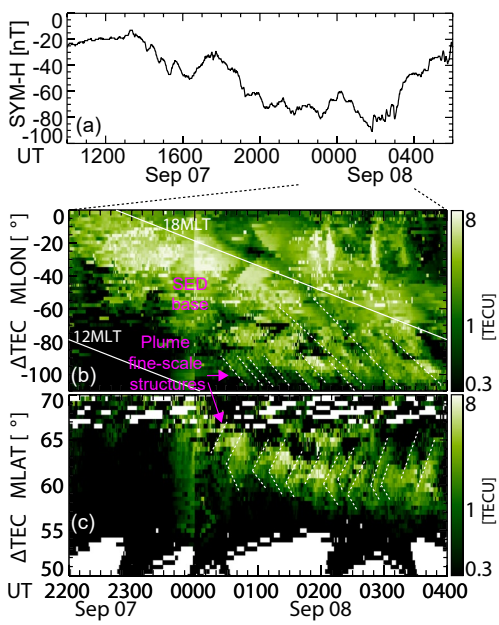

Figure 6. (a) SYM-H, (b) Δtotal electron content (TEC) along the plume as a function of magnetic longitude, and (c) ΔTEC as a function of magnetic latitude at −94° to −91° MLON.

comparable to the averaged sunward $E \times B$ drift speed that was detected at RBSP-A (Figure 2d). Therefore, the TEC observations provided the 2-d imaging of the fine-scale plume density.

While GPS receiver coverage above ~60° MLAT is generally sparse, southern Alaska has dense receiver coverage and allows us to resolve even smaller-scale density structures. Augustine Island in Alaska (59.3° latitude and −153° longitude in geographic; marked in Figure 5c) has 5 GPS receivers with short (<10 km) baselines, which can potentially resolve ~10s of km TEC structures. Looking from the Augustine Island GPS receivers, one of the GPS satellites (Pseudo-Random Noise (PRN) 04) was located at ~76° elevation and ~8° away from the magnetic field line at 03:55 UT on September 8. Thus, the GPS receivers were ideal to resolve TEC structures across the magnetic field. Figure 7a shows the geometry of the pierce points at 350 km altitude between the GPS receivers and PRN 04 at 03:55:49 UT. The time-series of the TEC at one of the GPS receivers (AV20) is shown in Figure 7g. TEC overall increased until ~03:54 UT and then decreased until ~04:30 UT. The elevated TEC corresponds to the plume. The TEC in the plume had fine-scale TEC structures that were also seen in Figure 5, and the amplitude of the TEC fluctuation reached ~30%–40% of the background TEC. The fine-scale TEC gradients in the plume that drifted at the convection speed were associated with the enhanced phase scintillation index (Figure 7h), indicating a significant impact of the fine-scale TEC structures on the GPS signal in the mid-latitude ionosphere (analogous to high-latitude scintillation Mitchell

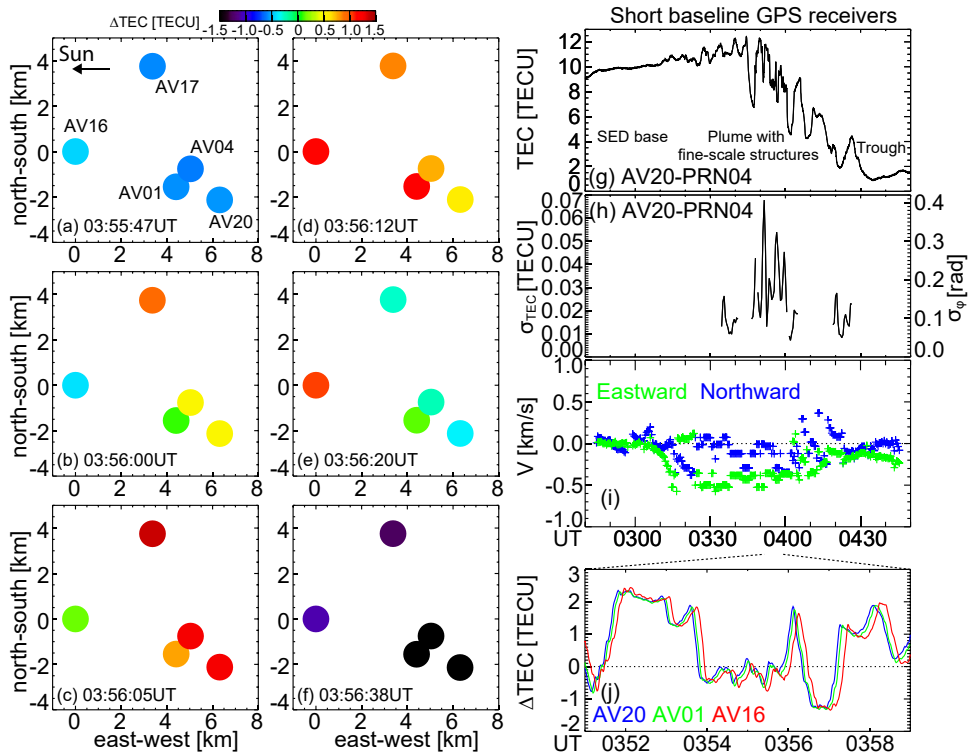

Figure 7. (a–f) Δtotal electron content (TEC) maps from the short-baseline global positioning system (GPS) receivers and pseudo-random noise (PRN) 04 on Augustine Island (see Figure 5c for the location) in the magnetic north-south and east-west distances relative to the AV16 pierce point at 350 km altitude. ΔTEC was obtained by detrending TEC over a 30 min period. (g) TEC and (h) phase scintillation index from the AV20 GPS receiver-PRN04 pair, (i) drift velocity of ΔTEC by triangulation of the GPS receivers, and (j) ΔTEC from AV20, AV01 and AV16 GPS receivers.

et al., 2005; Moen et al., 2013). Here, the phase scintillation was calculated using the method described in Mrak et al. (2020).

Figure 7j shows ΔTEC during the fine-scale TEC structures (03:51–03:59 UT) from three receivers that were aligned nearly with the orientation of the plume (southeast-to-northwest; AV20, AV01 and AV16). The fine-scale TEC structures at the three receivers were nearly identical except for the time lag, and thus they were spatial and drifted from southeast to northwest with little temporal variation. The drift of one of the fine-scale TEC structures is shown in Figures 7a–7f. TEC increased at the eastern receivers first (Figure 7b). The leading edge of the enhanced TEC moved westward (Figures 7c and 7d), the trailing edge of the enhanced TEC moved westward (Figure 7d), and then the TEC returned to the prior level (Figure 7f). The multipoint observations unambiguously resolved ~10 km scale TEC gradients whose normal direction was mainly in the east-west direction. The time lag of the TEC variations at the multiple points was also used to obtain the 2-d horizontal drift speed by a cross-correlation analysis (Figure 7i). The drift speed was dominantly westward with ~400–500 m/s speed. This speed is consistent with the TEC drift speed over a wider longitude range (Figure 6b), and its speed mapped to the magnetosphere (~4–5 km/s) was also comparable to the $E \times B$ drift speed at RBSP-A soon before 4 UT (Figure 2d) and at DMSP (Figure 3f).

2.5. Structured SAPS Flows in the Plume

The RBSP-A and DMSP observations in Figures 3 and 4 suggest that the flows in the plume were not uniform but highly variable. To identify whether the flow variations were moving spatial structures or temporal variations, we present observations from the SuperDARN radar at Christmas Valley West (CVW, 43.3° latitude and 239.6° longitude in geographic) in Figure 8. The radar field-of-view (FOV) covered the plume and the footprint of RBSP-A near the end of the main phase (Figure 8a).

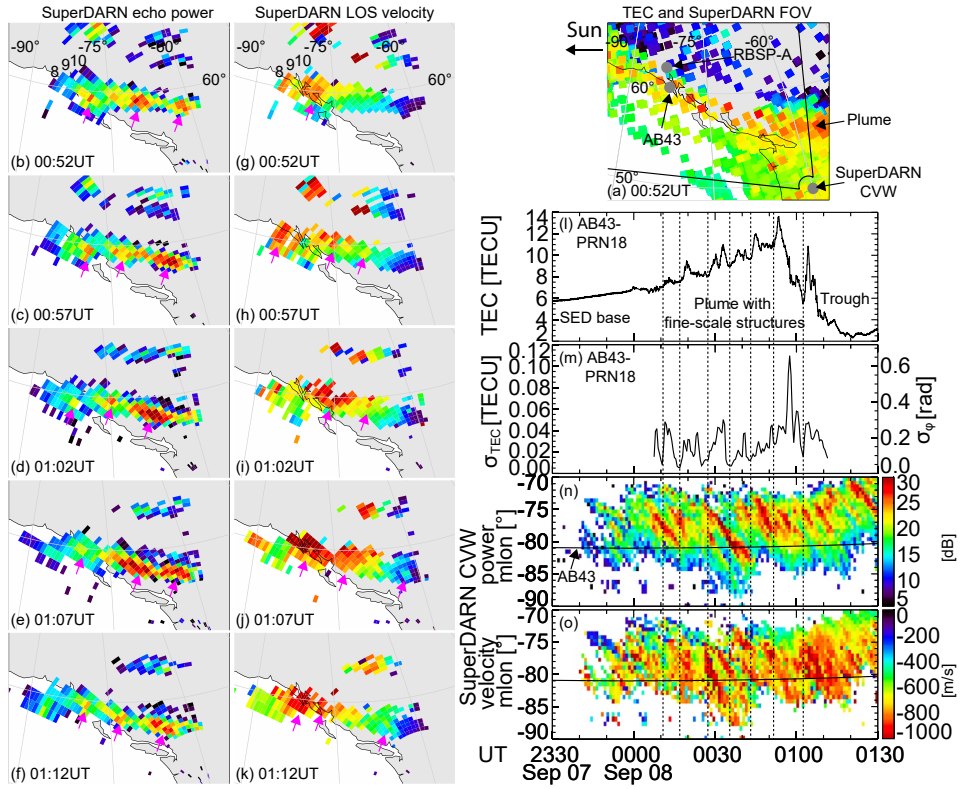

Figure 8. Super Dual Auroral Radar Network (SuperDARN) christmas valley west (CVW) radar and AB43 global positioning system (GPS) receiver data. (a) Radar field-of-view (FOV), AB43 GPS station and Van Allen Probes A (RBSP-A) footprint overlaid onto the total electron content (TEC) map at 00:52 UT on 8 September 2015. (b–f) Radar echo power, (g–k) lines-of-sight (LOS) velocity, (l) TEC and (m) phase scintillation index from the AB43 GPS receiver-PRN18 satellite pair, (n) radar echo power averaged over beam 8–10, and (o) LOS velocity averaged over beam 8–10. The solid lines in Panels n–o show the longitude of the pierce point of the AB43 receiver data. Only ionospheric echoes are used in the plots.

Selected snapshots of the SuperDARN echo power and LOS velocity are displayed in Figures 8b–8k. The radar echoes below ∼61° MLAT were located in or at the poleward edge of the plume. The backscatter echoes indicate existence of 10s-of-meter size density irregularities in the ionosphere (Nishitani et al., 2019). Thus, the radar echoes associated with the plume indicate that the plume contains density irregularities at 10s of m size, in addition to the 10–100s km size that were detected in TEC. The echo power was not constant across the radar beams but had a few peaks as highlighted by the arrows. Each region of the enhanced echo power had a ∼100 km size in north-south and ∼300 km size in east-west, and drifted sunward. The size and motion were comparable to the fine-scale TEC structures in the plume (Figure 5), indicating that the echo power structure corresponded to the fine-scale density in the plume.

The sunward-looking beams had the largest LOS velocity of ∼1 km/s, and the northward-looking beams measured much smaller velocity (Figures 8g–8k). This LOS velocity pattern corresponds to a sunward SAPS flow at ∼1 km/s. Interestingly, the LOS velocity also had localized enhancements that drifted sunward as highlighted by the arrows. The velocity enhancements were not evident along the northward-looking beams because of the large angle to the convection velocity, but the velocity enhancements became larger as the regions of the enhanced velocity drifted sunward. This observation indicates fine-scale structures of the SAPS flow. Some of the velocity enhancements were collocated with the enhanced echo power, but it was not always the case. The fine-scale SAPS flows are analogous to those reported by Makarevich and Bristow (2014), but the observation location was somewhat different. Their fine structures were observed near the poleward edge of the trough, while our fine-scale flow structures were seen in the plume equatorward of the trough.

Figures 8l–8m show the TEC and phase scintillation index from a GPS receiver (AB43) that was located within the radar FOV (Figure 8a). One of the GPS satellites (PRN 18) was located at ∼73° elevation and ∼5° away from

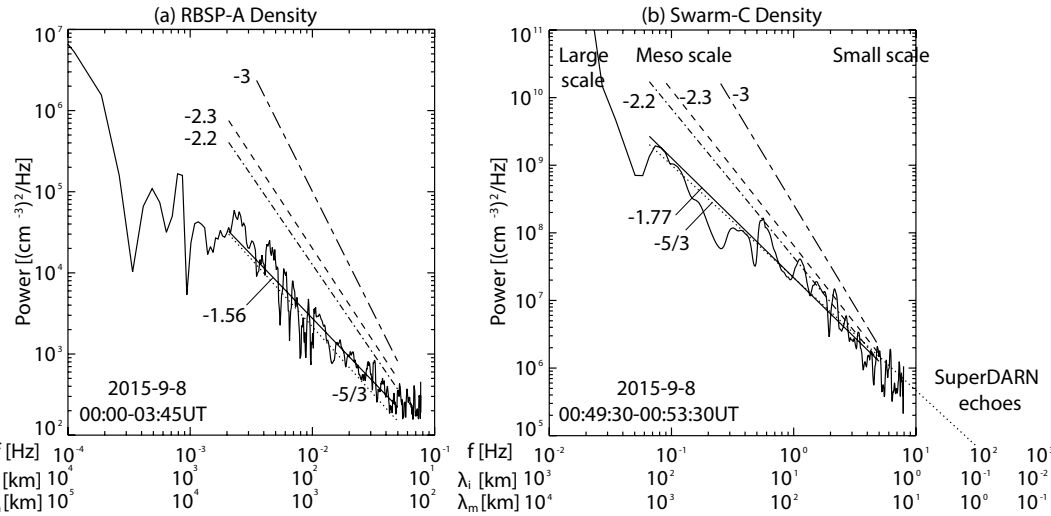

Figure 9. Power spectrum of the plasma density at (a) Van Allen Probes A (RBSP-A) (00:00–03:45 UT) and (b) Swarm-C (00:49:30–00:53:30 UT; same as the sixth orbit of Figure 4). The straight solid lines show power-law fitting. The dashed lines show the −5/3, −2.2, −2.3 and −3 power laws. The conversion to the wavelength at RBSP-A is obtained based on 8.4 km/s averaged flow speed (RBSP-A, Section 2.1).

the magnetic field in the main phase at 00:40 UT on September 8. The TEC structure at this location was similar to the one in Alaska in the early recovery phase (Figure 7g). The GPS receiver was in the SED base until ∼00 UT. The receiver encountered the plume with multiple TEC enhancements at ∼00:00–01:10 UT, and the enhanced phase scintillation index had a nearly one-to-one correspondence with the fine-scale TEC structures in the plume. Then the receiver went to the trough after ∼01:10 UT, where the density was much smoother than in the plume and scintillation was absent.

SuperDARN echo power and LOS velocity along the beams that were closest to the pierce point of the GPS receiver data (beams 08, 09 and 10) were averaged and are presented in Figures 8n–8o. The echo power and velocity have quasi-periodic (∼5 min) and coherent structures that moved away from the radar, that is, sunward along the plume. The enhancements of the echo power and velocity had nearly a one-to-one correspondence with the fine-scale TEC structures in the plume. This observation indicates that 10s of m irregularities were collocated with 10–100s of km fine-scale plume density structures and drifted sunward along the plume. The drift of the density irregularities was associated with the motion of the fine-scale SAPS flow structures (structures in Figures 8n–8o had the same slope). Hence, the quasi-periodic enhancements of the flow velocity may have contributed to form the fine-scale density enhancements. These observations indicate that the fine-scale SAPS flows contributed to form and transport the fine-scale density enhancements. The flow fluctuations at RBSP-A and DMSP were mainly spatial, where fine-scale SAPS flow structures repetitively drifted sunward and modulated the plume density.

2.6. Potential Mechanism of Density Irregularity Formation

The multi-scale nature of the plume plasma density in the magnetosphere and ionosphere can also be identified in the power spectra of the measured density. Figure 9a shows the power spectrum of the plasma density at RBSP-A at 00:00–03:45 UT (using data in Figure 2a). The power spectrum above ∼3 mHz (<∼5,000 km) followed a power law with a slope of ∼−1.56, and this scale of the density corresponded to the fine-scale density structures seen in Figure 3a. This slope was close to the −5/3 Kolmogorov spectrum, and thus suggests that Kolmogorov turbulence is the mechanism for creating the fine-scale density structures (Kolmogorov, 1991). The fine-scale density structures extend down to at least 100 km size in the magnetosphere (∼10 km in the ionosphere). The spectral power at ∼1,000 km size corresponds to the structures that were resolved by Moldwin et al. (1995), and the present study was able to show that the fine-scale density structures extend down at least to ∼100 km size. While we do not know the smallest size of the density due to the sampling frequency limit at RBSP, the Swarm

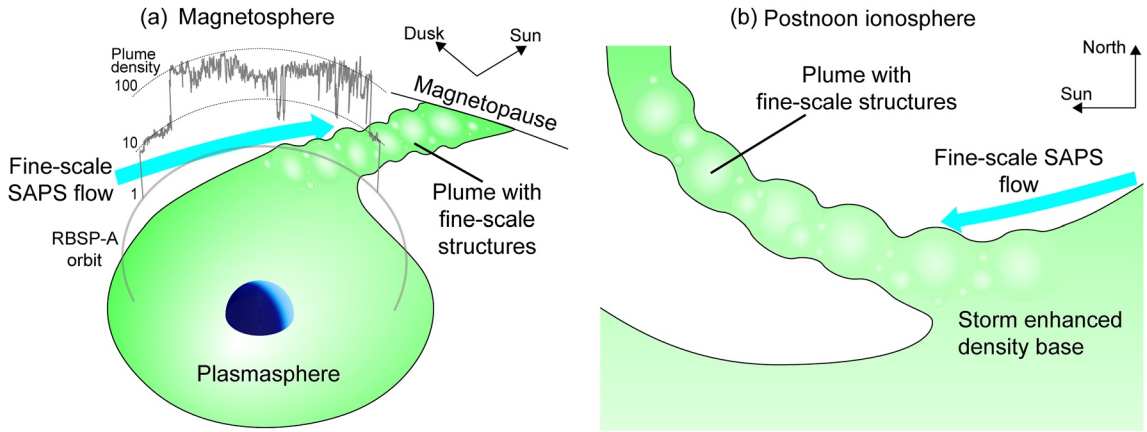

Figure 10. Schematic illustration of the multi-scale density in the plume in the (a) magnetosphere and (b) post-noon ionosphere. The green-to-white color indicates the density, and the light blue arrow denotes the fine-scale subauroral polarization streams flow. The gray color in Panel a shows the Van Allen Probes A orbit and the measured in-situ electron density.

density observations indicate that the slope continues down at least to ∼10 km size in the magnetosphere (∼1 km in the ionosphere).

Figure 9b replicates the power spectrum of the Swarm-C density at 00:49:30–00:53:30 UT from Figure 4j. The power law distribution above ∼0.1 Hz (<∼100 km in the ionosphere; <∼1,000 km in the magnetosphere) had a slope of ∼−1.77, which was also close to the −5/3 Kolmogorov spectrum. It suggests that the density irregularities in the ionosphere was also related to the Kolmogorov turbulence. Therefore, the fine-scale plume density structures in both the ionosphere and magnetosphere are suggested to form due to the turbulent SAPS flow.

The spectral slope is useful for evaluating whether other potential instability mechanisms are possible. The gradient drift instability is predicted to have a power law index of ∼−2.3 in the direction perpendicular to the convection (the Swarm satellite orbit was meridional and SAPS is nearly azimuthal) (Gondarenko & Guzdar, 2004). Kelvin-Helmholtz instability has a slope of ∼−2.2 across a flow channel (Huba et al., 1988), although the slope varies with the degree of magnetosphere-ionosphere coupling. A slope of ∼−3 is expected for 2-d enstrophy cascade (Hysell and Shume, 2002). Temperature gradient drift instability has a −2.2 slope (Eltrass et al., 2016). The measured spectral slope significantly deviates from those slopes. Hence, the Kolmogorov turbulence is the most likely scenario for driving the turbulence spectrum in the plume. The presence of turbulent flow has been demonstrated as fluctuating $E \times B$ drift speed at RBSP-A (Figure 2d) and localized flow structures in SuperDARN (Figure 8o).

The fine-scale density structures and their drift may be responsible for the enhanced phase scintillation index of the GPS receiver data (either as actual scintillation or as phase variation). While we do not know the spectrum below 1 km size in the ionosphere due to the sampling frequency limit, the enhanced SuperDARN echoes suggest that density irregularities in the plume may extend down at least to 10s of m scale.

3. Conclusion

We examined the multi-scale nature of the plasmaspheric plume density using multi-instrument observations in the magnetosphere and ionosphere during the 7–8 September 2015 geomagnetic storm. The large-scale TEC plume structure showed the typical plume evolution, and was overall consistent with the PTP model prediction. The TEC plume location mapped to the magnetosphere roughly agreed with the in-situ plume observation by RBSP-A, and the plume TEC along the RBSP-A footprint was proportional to the in-situ density. Thus, the TEC distribution in the ionosphere represents the plasmaspheric plume structure, and TEC may be useful for specifying the large-scale plume density distribution in the magnetosphere.

The key findings on fine-scale density structures in the plume are schematically illustrated in Figure 10. Both in situ density and TEC in the plume had large-amplitude fluctuations that were comparable to the magnitude of the large-scale plume density. The GPS receiver network was able to image the 2-d structure of the fine-scale density

as blobs with a characteristic size of ∼300 km and a sunward drift speed of ∼500–800 m/s along the plume in the ionosphere (∼3,000 km size and ∼5–8 km/s speed in the inner magnetosphere). The short-baseline GPS receiver network revealed even smaller (∼10 km) TEC gradients that drifted sunward at a similar speed. The fine-scale TEC structures were associated with the elevated phase scintillation index, and thus the fine-scale structures have a significant impact on radio signals.

The SuperDARN radar observations in the plume also identified that the SAPS flow in the plume had fine-scale (∼300 km) structures that drifted sunward along the plume. Therefore, the large-amplitude fluctuations of the $E \times B$ drift in the plasmaspheric plume are likely spatial structures. The echo power also had sunward-propagating fine-scale structures, and they had a nearly one-to-one correspondence with the fine-scale TEC structures, indicating that density irregularities in the plume continued down to 10s of m size. The fine-scale SAPS flow structures were suggested to create the fine-scale plume density structures at the base of the plume and transport them sunward along the plume.

Multiple plume crossings by the Swarm-C satellite identified time evolution of density structures across multiple scales. The density structures developed at large-scales (>∼500 km in the ionosphere) in the early main phase. Meso-scale (∼100 km) density increased throughout the main phase. Small-scale (<∼100 km) density was not enhanced in the early main phase but increased in the late main phase. The density spectrum at meso- and small-scales followed a power law with a ∼−5/3 slope, indicating that the energy cascade followed the Kolmogorov turbulence.

The fine-scale plume density structures were also associated with whistler-mode wave intensity modulation. Electron precipitation above 10 keV and below 1 keV was detected in the fine-scale density structures, and scattering of trapped electrons by the whistler-mode waves was suggested to be the cause of the precipitation in the plume. The precipitation may contribute to localized ionospheric heating, SAPS velocity reduction, and conductance enhancements.

The coordinated observations of the plume were able to visualize the multi-scale structures and drift of the density and velocity in the plume, and their possible importance in magnetosphere-ionosphere coupling. The present study showed that ionospheric observations are useful for remote sensing of the plume structures across scales. This method could be applied to other multi-scale structures for identifying the size and motion of various types of structures.

Data Availability Statement

The RBSP, Swarm, SuperDARN, DMSP and TEC data were obtained through https://cdaweb.gsfc.nasa.gov/pub/data/rbsp/rbspa/ (l3 efw, l3 emfisis, l3 rbspice, l3 ect, and l4 emfisis), http://vt.superdarn.org/tiki-index.php?page=Examine%20Fit%20Contents, https://swarm-diss.eo.esa.int/#swarm%2FAdvanced%2FPlasma_Data%2F16_Hz_Faceplate_plasma_density%2FSat_C, www.openmadrigal.org (distributed ground based satellite receivers), and https://www.unavco.org/data/gps-gnss/gps-gnss.html (rinex). Data processing used SPEDAS-V3.1 (Angelopoulos et al., 2019).

Acknowledgments
This work was supported by NASA grant 80NSSC18K0657, 80NSSC20K0604, 80NSSC20K0725, 80NSSC21K1321, and 80NSSC20K1788, NSF grant AGS-1907698 and AGS-2100975, and AFOSR grant FA9559-16-1-0364. The PTP simulation run was supported by the Magnetospheric Multiscale mission and by Southwest Research Institute. QM and WL would like to acknowledge NASA grants 80NSSC20K0196 and 80NSSC20K0698, NSF grant AGS-1847818, and Alfred P. Sloan Research Fellowship FG-2018-10936. The Christmas Valley SuperDARN radars are supported by NSF grants AGS-1934997 and AGS-1341925. We thank the Coupling, Energetics, and Dynamics of Atmospheric Regions for the "Grand Challenge: Multi scale I-T system dynamics" workshop, and ISSI/ISSI-BJ for the "Multi-Scale Magnetosphere-Ionosphere-Thermosphere Interaction" workshop.

References

Angelopoulos, V., Cruce, P., Drozdov, A., Grimes, E. W., Hatzigeorgiu, N., King, D. A., et al. (2019). The space physics environment data analysis system (SPEDAS). *Space Science Reviews*, *215*(1), 9. https://doi.org/10.1007/s11214-018-0576-4

Borovsky, J. E., & Denton, M. H. (2008). A statistical look at plasmaspheric drainage plumes. *Journal of Geophysical Research*, *113*, A09221. https://doi.org/10.1029/2007ja012994

Chen, L., Thorne, R. M., Li, W., Bortnik, J., Turner, D., & Angelopoulos, V. (2012). Modulation of plasmaspheric hiss intensity by thermal plasma density structure. *Geophysical Research Letters*, *39*, L14103. https://doi.org/10.1029/2012GL052308

Eltrass, A., Scales, W. A., Erickson, P. J., Ruohoniemi, J. M., & Baker, J. B. H. (2016). Investigation of the role of plasma wave cascading processes in the formation of midlatitude irregularities utilizing GPS and radar observations. *Radio Science*, *51*, 836–851. https://doi.org/10.1002/2015RS005790

Erickson, P. J., Foster, J. C., & Holt, J. M. (2002). Inferred electric field variability in the polarization jet from Millstone Hill E region coherent scatter observations. *Radio Science*, *37*(2), 1–15. https://doi.org/10.1029/2000RS002531

Foster, J. C., Erickson, P. J., Coster, A. J., Goldstein, J., & Rich, F. J. (2002). Ionospheric signatures of plasmaspheric tails. *Geophysical Research Letters*, *29*(13), 1. https://doi.org/10.1029/2002GL015067

Foster, J. C., Erickson, P. J., Coster, A. J., Thaller, S., Tao, J., Wygant, J. R., & Bonnell, J. W. (2014). Storm time observations of plasmasphere erosion flux in the magnetosphere and ionosphere. *Geophysical Research Letters*, *41*, 762–822. https://doi.org/10.1002/2013GL059124

Foster, J. C., Erickson, P. J., Lind, F. D., & Rideout, W. (2004). Millstone Hill coherent-scatter radar observations of electric field variability in the sub-auroral polarization stream. *Geophysical Research Letters*, *31*, L21803. https://doi.org/10.1029/2004GL021271

Goldstein, J., Pascuale, S. D., Kletzing, C., Kurth, W., Genestreti, K. J., Skoug, R. M., et al. (2014). Simulation of Van Allen Probes plasmapause encounters. *Journal of Geophysical Research: Space Physics*, *119*, 7464–7484. https://doi.org/10.1002/2014JA020252

Goldstein, J., & Sandel, B. R. (2005). The global pattern of evolution of plasmaspheric drainage plumes. In J. L. Burch, M. Schulz, & H. Spence (Eds.), *Inner magnetosphere interactions: New perspectives from imaging* (p. 1). American Geophysical Union. https://doi.org/10.1029/159gm02

Goldstein, J., Sandel, B. R., Thomsen, M. F., Spasojević, M., & Reiff, P. H. (2004). Simultaneous remote sensing and in situ observations of plasmaspheric drainage plumes. *Journal of Geophysical Research*, *109*, A03202. https://doi.org/10.1029/2003JA010281

Gondarenko, N. A., & Guzdar, P. N. (2004). Plasma patch structuring by the nonlinear evolution of the gradient drift instability in the high-latitude ionosphere. *Journal of Geophysical Research*, *109*, A09301. https://doi.org/10.1029/2004JA010504

Heine, T. R. P., Moldwin, M. B., & Zou, S. (2017). Small-scale structure of the midlatitude storm enhanced density plume during the 17 March 2015 St. Patrick's Day storm. *Journal of Geophysical Research: Space Research*, *122*, 3665–3677. https://doi.org/10.1002/2016ja022965

Huba, J. D., Mitchell, H. G., Keskinen, M. J., Fedder, J. A., Satyanarayana, P., & Zalesak, S. T. (1988). Simulations of plasma structure evolution in the high-latitude ionosphere. *Radio Science*, *23*(4), 503–512. https://doi.org/10.1029/RS023i004p00503

Hysell, D. L., & Shume, E. B. (2002). Electrostatic plasma turbulence in the topside equatorial F region ionosphere. *Journal of Geophysical Research*, *107*(A10), 1269. https://doi.org/10.1029/2001JA000227

Kolmogorov, A. (1991). The local structure of turbulence in incompressible viscous fluid for very large Reynolds numbers. *Proceedings of the Royal Society of London Series A: Mathematical and Physical Sciences*, *434*, 9–13. https://doi.org/10.1098/rspa.1991.0075

Li, W., Shen, X.-C., Ma, Q., Capannolo, L., Shi, R., Redmon, R. J., et al. (2019). Quantification of energetic Electron precipitation driven by plume whistler mode waves, Plasmaspheric hiss, and exohiss. *Geophysical Research Letters*, *46*, 3615–3624. https://doi.org/10.1029/2019gl082095

Makarevich, R. A., & Bristow, W. A. (2014). Fine structure of subauroral electric field and electron content. *Journal of Geophysical Research: Space Physics*, *119*, 3789–3802. https://doi.org/10.1002/2014JA019821

Matsui, H., Darrouzet, F., Goldstein, J., Puhl-Quinn, P. A., Khotyaintsev, Y. V., Lindqvist, P.-A., et al. (2012). Multi-spacecraft observations of small-scale fluctuations in density and fields in plasmaspheric plumes. *Annales Geophysicae*, *30*(3), 623–637. https://doi.org/10.5194/angeo-30-623-2012

Mishin, E., & Blaunstein, N. (2008). Irregularities within subauroral polarization stream-related troughs and GPS radio interference at midlatitudes. In P. M. Kintner, A. J. Coster, T. Fuller-Rowell, A. J. Mannucci, M. Mendillo, & R. Heelis (Eds.), *Midlatitude ionospheric dynamics and disturbances* (pp. 291–295).

Mishin, E. V., & Burke, W. J. (2005). Stormtime coupling of the ring current, plasmasphere, and topside ionosphere: Electromagnetic and plasma disturbances. *Journal of Geophysical Research*, *110*, A07209. https://doi.org/10.1029/2005JA011021

Mitchell, C. N., Alfonsi, L., De Franceschi, G., Lester, M., Romano, V., & Wernik, A. W. (2005). GPS TEC and scintillation measurements from the polar ionosphere during the October 2003 storm. *Geophysical Research Letters*, *32*, L12S03. https://doi.org/10.1029/2004GL021644

Moen, J., Oksavik, K., Alfonsi, L., Daabakk, Y., Romano, V., & Spogli, L. (2013). Space weather challenges of the polar cap ionosphere. *Journal of Space Weather and Space Climate*, *3*, A02. https://doi.org/10.1051/SWSC/2013025

Moldwin, M. B., Thomsen, M. F., Bame, S. J., McComas, D., & Reeves, G. D. (1995). The fine-scale structure of the outer plasmasphere. *Journal of Geophysical Research*, *100*(A5), 8021–8029. https://doi.org/10.1029/94JA03342

Mrak, S., Semeter, J., Nishimura, Y., Baker, J. B. H., Koustov, A. V., Shepherd, S. G., et al. (2020). Leveraging geodetic GPS receivers for ionospheric scintillation science. *Radio Science*, *55*, e2020RS007131. https://doi.org/10.1029/2020RS007131

Nishimura, Y., Mrak, S., Semeter, J. L., Coster, A. J., Jayachandran, P. T., Groves, K. M., et al. (2021). Evolution of mid-latitude density irregularities and scintillation in North America during the 7–8 September 2017 storm. *Journal of Geophysical Research: Space Physics*, *126*, e2021JA029192. https://doi.org/10.1029/2021ja029192

Nishitani, N., Ruohoniemi, J. M., Lester, M., Baker, J. B. H., Koustov, A. V., Shepherd, S. G., et al. (2019). Review of the accomplishments of mid-latitude super dual auroral radar network (SuperDARN) HF radars. *Progress in Earth and Planetary Science*, *6*, 27. https://doi.org/10.1186/s40645-019-0270-5

O'Brien, T. P., Russell, P. C. T., Steinberg, J. T., Chao, J. K., Zastenker, G., Vaisberg, O. L., et al. (2003). Empirical plasmapause models from magnetic indices. *Geophysical Research Letters*, *30*(4), 1152. https://doi.org/10.1029/2002GL016007

Oksavik, K., Greenwald, R. A., Ruohoniemi, J. M., Hairston, M. R., Paxton, L. J., Baker, J. B. H., et al. (2006). First observations of the temporal/spatial variation of the sub-auroral polarization stream from the SuperDARN Wallops HF radar. *Geophysical Research Letters*, *33*, L12104. https://doi.org/10.1029/2006GL026256

Shue, J.-H., Song, P., Russell, C. T., Steinberg, J. T., Chao, J. K., Zastenker, G., et al. (1998). Magnetopause location under extreme solar wind conditions. *Journal of Geophysical Research*, *103*(A8), 17691–17700. https://doi.org/10.1029/98JA01103

Spasojević, M., Goldstein, J., Carpenter, D. L., Inan, U. S., Sandel, B. R., Moldwin, M. B., & Reinisch, B. W. (2003). Global response of the plasmasphere to a geomagnetic disturbance. *Journal of Geophysical Research*, *108*(A9), 1340. https://doi.org/10.1029/2003JA009987

Tsyganenko, N. A. (2002). A model of the magnetosphere with a dawn-dusk asymmetry, 1, Mathematical structure. *Journal of Geophysical Research*, *107*(A8). https://doi.org/10.1029/2001JA000219

Yuan, Z., Xiong, Y., Pang, Y., Zhou, M., Deng, X., Trotignon, J. G., et al. (2012). Wave-particle interaction in a plasmaspheric plume observed by a Cluster satellite. *Journal of Geophysical Research*, *117*, A03205. https://doi.org/10.1029/2011JA017152

Zhang, S.-R., Erickson, P. J., Coster, A. J., Rideout, W., Vierinen, J., Jonah, O., & Goncharenko, L. P. (2019). Subauroral and polar traveling ionospheric disturbances during the 7–9 September 2017 storms. *Space Weather*, *17*(1), 1748–1764. https://doi.org/10.1029/2019SW002325